OUKA
The University of Osaka
Institutional Knowledge Archive

Title	Long-term stability of nickel-based ohmic contacts with n-type and p-type 4H-SiC in a high-temperature environment
Author(s)	Masunaga, Masahiro; Crescitelli, Viviana; Funaki, Tsuyoshi
Citation	Japanese Journal of Applied Physics. 2020, 59(10), p. 104005
Version Type	AM
URL	https://hdl.handle.net/11094/78287
rights	The full-text file will be made open to the public on 9 October 2021 in accordance with the publisher's policy.
Note	

The University of Osaka Institutional Knowledge Archive : OUKA

https://ir.library.osaka-u.ac.jp/

The University of Osaka

Long-term Stability of Nickel-based Ohmic Contacts with n-type and p-type 4H-SiC in a High-temperature Environment

Masahiro Masunaga[1, 2*], Viviana Crescitelli[2], and Tsuyoshi Funaki[1]

[1]*Division of Electrical, Electronic and Information Engineering, Graduate School of Engineering, Funaki Laboratory, Osaka University, 2-1 Yamadaoka, Suita, Osaka 565-0871, Japan*

[2]*Center for Technology Innovation – Electronics, Research & Development Group, Hitachi, Ltd., 1-280 Higashi-koigakubo, Kokubunji-shi, Tokyo 185-8601, Japan*

[*]E-mail: masahiro.masunaga.fw@hitachi.com

Abstract

Long-term thermal stability of specific contact resistance (ρ_c) in cross-bridge kelvin resistors (CBKRs), with an Al/TiN/Ti/Ni_2Si/4H-SiC layered structure was studied. In high-temperature-storage tests at 500°C, ρ_c of p-type SiC increased after it decreased to 1/100 from its initial value; however, in high-temperature-storage tests at 300°C, it was stable up to 1000 hr. The initial decline of ρ_c was due to formation of titanium-silicide alloy, whose barrier height is lower than that of Ni_2Si phase. It was found that ρ_c increased when the aluminum electrode disappeared because aluminum displaced silicon in the silicon-dioxide layer. In thermal-shock tests (-40°C/300°C), ρ_c hardly changed up to 2000 cycles, and that trend was constant regardless of SiC carrier type. In both tests, almost no thermal deterioration of ρ_c around 300°C was observed even in air, so it is concluded that the CBKR structure is robust enough for installation in a high-temperature environment such as a nuclear power plant under decommissioning.

1. Introduction

Power devices and sensors are indispensable for operation, control, and safety of robots used in decommissioning nuclear power plants. Silicon (Si)-based devices are conventionally used for actuator drivers and sensors. However, they are susceptible to radiation and high temperature, so they require extra measures for normal operation (such as shielding or protection circuits).

Silicon-carbide (SiC) is a promising semiconductor material for devices operating in high-radiation[1-7] and high-temperature[8-13] environments. In a previous work, the authors fabricated a SiC operational amplifier (op-amp) based on 4H-SiC complementary MOS (CMOS) technology[6]. The developed device showed superior radiation resistance (over 1 MGy), without use of a shield or an external process such as thermal annealing, due to significantly decreased interface state density of the 4H-SiC MOS with nitric-oxide (NO) passivation[5]. The operation of SiC-CMOS integrated circuits in high-temperature environments has been demonstrated[14-16]. The experimentally demonstrated long-term reliability of a gate-oxide film suggested a maximum operating electric field of 3.9 MV/cm for a 100-year lifetime at 375°C[17].

However, a contact metal and capping layer with high temperature resistance (at 300°C or more) suitable for SiC-CMOS has not been sufficiently studied. Nickel (Ni) has been frequently studied as a contact metal for n-type SiC[18-21], and its barrier height (ϕ_B) is known to decrease from 1.60 eV to 0.45 eV after annealing at over 900°C[21,22]. This ohmic behavior can be mainly attributed to (i) formation of a silicide such as Ni_2Si and/or (ii) redistribution of interfacial carbon after the silicide formation and its movement from the interface towards the contact surface at elevated temperature[20]. Also, some researchers consider that carbon vacancies are generated from outdiffusion of carbon atoms at the interface during annealing, and those carbon vacancies act as donors that play a key role in reducing effective ϕ_B and promoting formation of ohmic contacts[19]. Stacked titanium and aluminum has been studied as contact metal for p-type SiC[23-25]. Interface alloys such as Al_3Ti and Ti_3SiC_2 are produced at the interface between the titanium/aluminum metal stack and the p-type SiC during high-temperature annealing, and the Ti_3SiC_2 divides the high ϕ_B of the metal/p-type SiC contact interface into two low ϕ_B to reduce ρ_c[25,26]. Because of that fact, it is desirable to apply different contact metals to n-type and p-type SiC, although the CMOS manufacturing process becomes complicated.

Forming ohmic contacts to both n-type and p-type regions by the same process has been studied in the CMOS fabrication[27-32]. Linear-transmission-line-model samples, which have

Ni-based ohmic contacts to implanted n-type and p-type SiC, showed ρ_c in the range of 10^{-6} Ωcm^2 and 10^{-3} Ωcm^2, respectively at room temperature[31]. Furthermore, the samples demonstrated high thermal stability in nitrogen atmosphere[32]. However, in these studies, oxidation of the contacts in air was not considered. Contact resistance increased 10 times from the initial value in air at 300°C for a device with Ni-based ohmic contacts[33].

To address the oxidation issue, a conductive diffusion barrier that can prevent diffusion of oxygen into the contact metal has been suggested[34-39]. A conductive diffusion barrier, such as TaRuN[36,37] and TiN[38,39], is formed between the contact metal and the capping layer to slow the diffusion of oxygen and/or the reaction of oxygen with the contact metal and capping layer. The experimentally demonstrated performance of conductive diffusion barrier with TaRuN changed contact resistance only slightly from 2×10^{-5} Ωcm^2 to 3×10^{-5} Ωcm^2 for 2000 hr in air over 300°C[36]. However, patterning the noble metals such as ruthenium in CMOS processing is not straightforward, and substitution to TiN is desired. In addition, although thermal stability of these stacked structures have been studied frequently, the influence of delamination caused by Kirkendall voids, which are formed at the interface between a Ni-based contact and the SiC substrate[40], has not been sufficiently verified.

This study subjects 4H-SiC cross-bridge kelvin resistors (CBKRs), with an Al/TiN/Ti/Ni silicide/4H-SiC layered structure, to a high-temperature-storage test in air and a specific environment. And this study subjects to a thermal-shock test to verify ρ_c fluctuation due to delamination of contact metals. To check deterioration of the interface, ρ_c in the case of implanted n-type and p-type SiC layer is periodically sampled.

2. Experimental methods

The CBKR samples (NN05 and PP10) investigated in this work were fabricated in-house as n-type and p-type semiconductors, respectively. Their detailed specifications are listed in Table I. Plan views and cross sections of NN05 and PP10 are shown in Figs. 1 and 2, respectively. The samples were monolithically fabricated on an n-type 4H-SiC epitaxial layer doped with nitrogen at 7×10^{14} cm^{-3} and grown on a 4H-SiC substrate that was 4° off the silicon face. Acceptor concentration of a p-well in NN05 (3.6×10^{17} cm^{-3}) was formed by aluminum implantation. An n+ layer in NN05 and a p+ layer in PP10 were formed by ion implantation. The ion species was nitrogen for n-type and aluminum for p-type. After the impurities were implanted, the samples were activated by annealing at 1700°C. Then, a silicon-dioxide (SiO_2) interlayer was deposited on the SiC epitaxial surface by chemical vapor deposition, and the CKBR patterns were formed with a photoresist. After a part of the

SiO_2 interlayer was removed, the exposed surface of the 4H-SiC epitaxial layer was cleaned by buffered hydrofluoric acid. A 55-nm-thick nickel layer deposited on the exposed surface was annealed at 1000°C for silicidation. Titanium (10 nm), TiN (30 nm), and aluminum (300 nm) films were deposited on the nickel-silicide layer by sputtering as an adhesion-promoting layer, a conductive diffusion barrier and a capping layer, respectively. Finally, a SiO_2 layer was formed to passivate them, and ρ_c of the fabricated samples was measured with a precision semiconductor parameter analyzer (4156B, Keysight Technologies, Inc.). The basic experimental setup for the measurement is shown in Fig. 2(a), and ρ_c was measured by four-terminal Kelvin sensing with the current measured at "source-measurement unit 1" (SMU1) and the difference between voltages measured at "voltage-meter unit 1" (VMU1) and VMU2 as shown in Fig. 3. ρ_c was average of contact resistance from -1 V to 1 V except 0 V, and temperature dependence of ρ_c in the range 25–500°C was studied.

The high-temperature-storage-test samples were heated in specific environments (400°C and 500°C) in an electric furnace (DD-93000C, Kokusai Electric co., Ltd.) filled with nitrogen gas or at 300°C in a vacuum chamber (ZXVC-10150HT, Vector Semiconductor co., Ltd.). All the samples were tested in wafer state. Specific contact resistance (ρ_c) of the samples heated at 400°C and 500°C test was periodically sampled at room temperature by taking the samples out of the electric furnace. In contrast, ρ_c of the sample heated at 300°C test was continuously measured by probe in the vacuum chamber for 1000 hr.

Long-term thermal stability of CBKRs in air was evaluated using the samples, which were attached to a ceramic package, as shown in Fig. 4, with gold-germanium solder to withstand extreme temperature storage and temperature change of the thermal-shock test[41]. The sample and terminals of the ceramic package were connected by aluminum wires. The samples subjected to thermal-shock tests at temperature difference (ΔT) of 340°C for 2000 cycles were set in a thermal-shock chamber (TSE-11, Espec corp.) with a temperature range of -40°C to 300°C. The temperature sequence—in which the temperature was transitioned at higher than 68°C per minute—is shown in Fig. 5.

Before the thermal-shock test, peel strength of the aluminum wires was tested by bond tester (Condor Sigma, XYZTEC, Inc.). The normal distribution of the wire's peel fracture strength before and after the thermal-shock test is shown in Fig. 6. It is clear from the figure that the wire's peel fracture strength is significantly decreased by metal fatigue. However, all tested wires (20 in total) keep contacts and their mechanical strengths were over 0.92 gf for 2000 cycles. The influence of wire-bond deterioration on ρ_c is negligible for 2000 cycles.

3. Results and discussion

3.1 Temperature dependence of contact resistance

Before high-temperature storage tests, as temperature dependence of ρ_c for NN05 and PP10 are shown in Figs. 7(a) and 7(b). Specific contact resistance (ρ_c) of NN05 stares in the range of 10^{-6} Ωcm^2 up to 500°C. In contrast, ρ_c of PP10 fluctuates in the range from 10^{-2} Ωcm^2 at 25°C to 10^{-4} Ωcm^2 at 500°C. The difference in temperature dependences of ρ_c between NN05 and PP10 indicates different mechanism in carrier transport at the interface. The carrier-transport mechanism is related to the Padovani-Stratton parameter (E_{00})[26,34] and depends on both temperature and doping level. Ratio E_{00}/kT (where k is the Boltzmann constant and T is temperature) indicates the carrier transport for which a specific current-flow mechanism plays the dominant role[26,34].

According to ratio E_{00}/kT, carrier transport of NN05 is governed by a field-emission (FE) model. The extracted value of ϕ_B is 0.5 eV, which agrees with its value of Ni_2Si contact to n-type SiC under a similar implantation and annealing condition[32]. On the other hand, carrier transport of PP10 is governed by a thermionic-field-emission (TFE) model, and the value of ϕ_B is calculated as 1.1 eV, which is 0.35 eV higher than that of the reported Ni_2Si contact to p-type SiC[32]. For p-type material, ϕ_B is often found to be independent of the metal work function and is related to the density of interface states (D_{it})[26,48,49]. ϕ_B for p-type material (ϕ_{BP}) can be derived approximately based on Bardeen model as[26,48,49]

$$\phi_{BP} = -\gamma(\phi_m - \chi) - (1-\gamma)(E_g - \phi_0) + E_g \quad (1)$$

where γ is the pinning factor related to the D_{it}, ϕ_0 is the charge-neutrality level, ϕ_m is work function of metal, χ is the electron affinity of SiC, and E_g is band gap. γ ranges from 0 to 1. Sufficiently high D_{it} (γ is close to 0) induces Fermi level pinned at the ϕ_0 in the band gap, and it reduces contact resistance[26,42]. On one hand, at low D_{it}, the ϕ_{BP} subjects to Schottky-Mott model[26]. Thus, D_{it} is key factor for ϕ_{BP}. However, D_{it} is known to be strongly influenced by surface treatments prior to SiC metalization[26]. It is considered that the difference of surface pretreatments made the difference in ϕ_{BP} in this case.

The constitution of contact metal in the PP10 sample was analyzed by XRD (X-ray diffraction). The result of XRD is shown in Fig. 8. In the PP10 sample, the Ni_2Si phase was formed at the metal/SiC interface.

3.2 High-temperature-storage test in specific environments

Specific contact resistance (ρ_c) of NN05 and PP10 was investigated to evaluate the

deterioration of the interface between the contact metal and SiC layer in the high-temperature-storage test. The high-temperature-storage test was performed in vacuum or nitrogen atmosphere to exclude the influence of oxidation. ρ_c of NN05 and PP10 for storage time is plotted in Figs. 9(a) and 9(b), respectively. Note that ρ_c of NN05 stored at 300°C in the aging-time range of 450 to 600 hr was lost due to probing error. And ρ_c of NN05 stored at 500°C monotonically increases until 575 hr, even though it hardly changes in the 300°C and 400°C storage tests. On the contrary, ρ_c of PP10 shows a different thermal property from that of NN05 as in Fig. 9(b). That is, ρ_c of PP10 stored at 500°C increases after it decreased to 1/100 of its initial value.

The cross-section of PP10 was observed to investigate the cause of the large variation of ρ_c. TEM images before and after the 500°C storage test are shown in Figs. 10(a) and 10(b), respectively. Ni_2Si, titanium, and TiN were present between the aluminum electrode and SiC layer in the initial state as shown in Fig 10(a). SiO_2 was present on the aluminum electrode as a passivation layer. Carbon clusters agglomerated in the Ni_2Si layer far from interface. After the 500°C/575 hr storage test, the aluminum electrode disappeared or a part of it became discolored as shown in Fig. 10(b). In addition, the SiO_2 layer appeared to be deformed. The condition of the Ni_2Si phase between the TiN and the SiC layers was also changed during the high-temperature storage test; that is, the carbon clusters disappeared.

The elemental analysis was performed at points 1, 2, and 3 in Fig. 10(b). Results of TEM-EDX at points 1, 2, and 3 are shown in Figs. 11, 12, and 13, respectively. It is noted for Ga peaks is caused by ion source of focused ion beam (FIB), and Cu peaks is caused by our sample holder. The predominant aluminum and oxygen peaks are found for point 1. Aluminum is known to displace silicon in the SiO_2 structure and form an Al-O compound with Al:O concentration ratio between 1:1 and 1.3:1 at temperature near 500°C[43)]. Furthermore, this displacement reaction penetrates deeply into the SiO_2 structure without a noticeable change in the rate of penetration[43)]. In other words, the aluminum electrode steadily disappeared via a solid-state chemical reaction with high-temperature-storage time, and ρ_c gradually increased simultaneously.

The predominant silicon and titanium peaks, as well as subordinate nitrogen, aluminum, and carbon peaks, are found (although nickel is not detected) for point 2. This result indicates a chemical reaction in silicide from Ni_2Si phase to titanium-silicide alloy. It also shows aluminum atoms slightly penetrate into the silicide layer through TiN. From ρ_c in Fig. 9(b), ϕ_B of the titanium-silicide alloy is estimated as 0.82 eV, which agrees with ϕ_B of the titanium-alloy contact to p-type SiC[44)]. In the same way, from ρ_c in Fig. 9(a), ϕ_B of NN05 after the

high-temperature-storage test is estimated as 0.73 eV, with agrees with ϕ_B of the titanium ohmic contact on n-type SiC, which was formed by low-temperature anneal[45]. Titanium silicide formed below 600°C is mainly composed of Ti_5Si_4, Ti_5Si_3, and TiC[45], and these alloys constitutes for low ohmic contact to p-type SiC.

The nickel and silicon subordinate peaks are found for point 3 in addition to a predominant aluminum peak, as shown in Fig. 13. The nickel atoms penetrate into the aluminum-layer side (accompanied by silicon atoms) through TiN, and disappeared from the silicide layer during the high-temperature-storage test. An AlSiNi alloy is then formed in the aluminum region.

Thus, Fig. 9(b) can be interpreted as follows. From 0 to 200 hr, Ni_2Si phase transformed to titanium-silicide alloy and ρ_c was reduced due to reduction of ϕ_B. After that, ρ_c was increased because the aluminum electrode diffused to SiO_2 structure and vanished. Same phenomenon is expected to occur in ρ_c of NN05. In the period from 0 to 200 hr, ρ_c was increased due to elevation of ϕ_B in n-type material of the titanium-silicide alloy. And then, disappearance of aluminum electrode further increased ρ_c of NN05.

3.3 Long-term thermal stability in air

To investigate deterioration of ρ_c of NN05 and PP10 by oxidation and delamination, the NN05 and PP10 samples were subjected to high-temperature-storage tests and thermal-shock tests in air. Storage temperature was set in 300°C to suppress ρ_c variation due to aluminum diffusion from the capping layer and change in the silicide composition. In Fig. 14, ρ_c of NN05 and PP10 against storage time is plotted. In addition, ρ_c of a reported device with Ni-based ohmic contact to n-type SiC without the diffusion barrier in Ref. 33 is also shown for comparison. NN05 shows ρ_c hardly changes up to 1000 hr because TiN prevents diffusion of oxygen into the metal/SiC interface[37] although ρ_c of the reported device in Ref. 33 increases 10 times from the initial value. On the other hand, ρ_c of PP10 at 400 hr becomes 1.7 times larger than the initial value. After 400 hr, ρ_c saturates. This result agrees with that for ρ_c in vacuum condition, as shown in Fig. 9(b). It is considered that influence of oxidation in Ni_2Si is negligible because there is no difference in ρ_c between Fig. 9(b) and Fig. 14.

Increase of ρ_c in PP10 during the high-temperature-storage test has two main causes: (i) reduction of aluminum concentration at interface and (ii) ϕ_B for p-type material increase due to silicide transformation. A thermally induced interaction between thin-film aluminum and Ni silicide is known to occur at 275°C, and the interaction forms NiAl silicide alloy[46].

If the similar phenomenon occurs at the interface, the NiAl silicide alloy is assumed to reduce ϕ_B due to its high work function[47]. Thus, increase of ρ_c is likely due to (i), and detailed investigation is our future work.

In Fig. 15, ρ_c of NN05 and PP10 is plotted for number of thermal-shock cycles. It is clear that ρ_c after the thermal-shock tests show the same tendency as that shown in Fig. 14. As for NN05, ρ_c hardly changes up to 2000 cycles, as for PP10, ρ_c slightly increases up to 1200 cycles and then saturates. The influence of the delamination caused by Kirkendall voids is supposed to be small regardless of carrier type at ΔT= 340°C because ρ_c variation of NN05 and PP10 is same or small in comparison with it in the high-temperature-storage tests. In other words, the effect of accumulated fatigue by large temperature change at the interface between the metal and SiC layers is negligible.

4. Conclusions

Long-term thermal stability of specific contact resistance (ρ_c) in cross-bridge kelvin resistors (composed of Al/TiN/Ti/Ni_2Si/4H-SiC) at high temperature was studied. In high-temperature-storage tests, ρ_c for p-type SiC stored at 500°C increased after it decreased to 1/100 from the initial value, though that increase does not occur for 300°C storage up to 1000 hr. The initial decline of ρ_c was due to formation of titanium-silicide alloy, whose barrier height is lower than that of Ni_2Si. Moreover, ρ_c increased with disappearance of the aluminum electrode, stemming from aluminum displacement into the silicon-dioxide layer. These results indicate that the aluminum electrode should be changed to a metal one with excellent heat resistance (such as molybdenum) or be covered with a barrier metal for operation at high temperature around 500°C. They also indicate that switching the silicide material from a nickel-based to a titanium-based one improves thermal stability of ρ_c. In thermal-shock tests (-40°C/300°C), ρ_c hardly changed up to 2000 cycles regardless of SiC carrier type. In both tests, almost no thermal deterioration of ρ_c around 300°C was observed even in air, and stable operation of cross-bridge kelvin resistors can be expected up to 300°C.

References

1) M. Yoshikawa, H. Itoh, Y. Morita, I. Nashiyama, S. Misawa, H. Okumura, and S. Yoshida, J. Appl Phys. **70** (1991) 1309.
2) K. K. Lee, T. Ohshima, and H. Itoh, IEEE Trans. Nucl. Sci. **50** (2003) 194.
3) A. Akturk, J. M. McGarrity, S. Potbhare, and N. Goldsman, IEEE Trans. Nucl. Sci. **59** (2012) 3258.
4) S. K. Dixit, S. Dhar, J. Rozen, S. Wang, R. D. Schrimpf, D. M. Fleetwood, S. T. Pantelides, J. R. Williams, and L. C. Feldman, IEEE Trans. Nucl. Sci. **53** (2006) 3687.
5) T. Chen, Z. Luo, J. D. Cressler, T. F. Isaacs-Smith, J. R. Williams, G. Chung, and S. D. Clark, Solid-State Electron., **46** (2002) 2231.
6) M. Masunaga, S. Sato, R. Kuwana, N. Sugii, and A. Shima, IEEE Trans. Electron Devices, **67** (2020) 224.
7) S. Saveda, S. Kuroki, L. Lanni, R. Hadayati, T. Ohshima, T. Makino, A. Hallen, and C. M. Zetterling, IEEE Trans. Nucl. Sci. **64** (2017) 852.
8) T. Funaki, J. C. Balda, J. Junghans, A. S. Kashyap, H. A. Mantooth, F. Barlow, T. Kimoto, and T. Hikihara, IEEE Trans. Power Electron., **22** (2007) 1321.
9) M. Okamoto, T. Yatsuo, K. Fukuda, and H. Okumura, Jpn J. Appl. Phys. **48** (2009) 04C087.
10) R. Ghandi, C. P. Chen, L. Yin, X. Zhu, L. Yu, S. Arthur, F. Ahmad, and P. Sandvik, IEEE Electron Device Lett., **35** (2014) 1206.
11) S. Roy, R. C. Murphree, A. Abbasi, A. Rahman, S. Ahmed, J. A. Gattis, A. M. Francis, J. Holmes, H. A. Mantooth, and J. Di, IEEE Trans. Ind. Electron., **64** (2017) 8364.
12) M. Ekstrom, B. G. Malm, and C. M. Zetterling, IEEE Electron Device Lett., **40** (2019) 670.
13) M. Nakajima, M. Kaneko, and T. Kimoto, IEEE Electron Device Lett., **40** (2019) 866.
14) D. B. Slater, G. M. Johnson, L. A. Lipkin, A. V. Survorov, and J. W. Palmour, in Proc. 3rd Int. High-Temperature Electron. Conf., (1996) XI-17.
15) A. Rahman, S. Roy, R. Murphree, R. Kotecha, K. Addington, A. Abbasi, H. A. Mantooth, A. M. Francis, J. Holmes, and J. Di, IEEE J. Emerging Sel. Topics Power Electron., **4** (2016) 935.
16) D. T. Clark, E. P. Ramsay, A. E. Murphy, D. A. Smith, R. F. Thompson, R. A. R. Young, J. D. Cormack, C. Zhu, S. Finney, and J. Fletcher, Mater. Sci. Forum, **679-680** (2011) 726.
17) L. C. Yu, G. T. Dunne, K. S. Matocha, K. P. Cheung, J. S. Suehle, and K. Sheng, IEEE Trans. Device Mater. Rel., **10** (2010) 418.
18) Lisa M. Porter, and Robert F. Davis, Mater. Sci. Eng. B **34** (1995) 83.
19) Sang Youn Han, Ki Hong Kim, Jong Kyu Kim, Ho Won Jang, Kwang Ho Lee, Nam-Kyun

Kim, Eun Dong Kim, and Jong-Lam Lee, Appl. Phys. Lett. **79** (2001) 1816.

20) F. La Via, F. Roccaforte, V. Raineri, M. Mauceri, A. Ruggiero, P. Musumeci, L. Calcagno, A. Castaldini, and A. Cavallini, Microelectron. Eng. **70** (2003) 519.
21) A. V. Kuchuk, P. Borowicz, M. Wzorek, M. Borysiewicz, R. Ratajczak, K. Golaszewska, E. Kaminska, V. Kladko, and A. Piotrowska, Adv. Condens. Matter Phys. **2016** (2016) 9273702.
22) Sang Youn Han and Jong-Lam Lee, J. Electrochem. Soc. **149** (2002) G189.
23) C. A. Fisher, M. R. Jennings, Y. K. Sharma, A. Sanchez-Fuentes, D. Walker, P. M. Gammon, A. Perez-Tomas, S. M. Thomas, S. E. Burrows, and P. A. Mawby, International journal of Fundamental Physical Sciences (IJFPS), **4** (2014) 95.
24) A. Frazzetto, F. Giannazzo, R. L. Nigaro, V. Raineri, and F. Roccaforte, J. Phys. D: Appl. Phys. **44** (2011) 255302.
25) Brian J. Johnson and Michael A. Capano, J. Appl. Phys. **95** (2004) 5616.
26) Lingqin Huang, Mali Xia, and Xiaogang Gu, J. Cryst. Growth, **531** (2020) 125353.
27) H. Shimizu, A. Shima, Y. Shimamoto, and N. Iwamuro, Jpn J. Appl. Phys. **56** (2017) 04CR15.
28) K. Buchholt, R. Ghandi, M. Domeij, C. -M. Zetterling, J. Lu, P. Eklund, L. Hultman, and A. Lloyd Spetz, Appl. Phys. Lett. **98** (2011) 042108.
29) K. Ito, T. Onishi, H. Takeda, K. Kohama, S. Tsukimoto, M. Konno, Y. Suzuki, and M. Murakami, J. Electron. Mater. **37** (2008) 1674.
30) S. Tsukimoto, T. Sakai, T. Onishi, K. Ito, and M. Murakami, J. Electron. Mater. **34** (2005) 1310.
31) S. Tanimoto, N. Kiritani, M. Hoshi, and H. Okushi, Mater. Sci. Forum, **389** (2002) 879.
32) M. Vivona, G. Greco, F. Giannazzo, R. Lo Nigro, S. Rascuna, M. Saggio, and F. Roccaforte, Semicond. Sci. Technol. **29** (2014) 075018.
33) A. Virshup, L. M. Porter, D. Lukco, K. Buchholt, L. Hultman, and A. L. Spetz, Journal of Electronic Materials, 38 (2009) 569.
34) Z. Wang, W. Liu, and C. Wang, J. Electron. Mater. **45** (2016) 267.
35) S. Liu, Z. He, L. Zheng, B. Liu, F. Zhang, L. Dong, L. Tian, Z. Shen, J. Wang, Y. Huang, Z. Fan, X. Liu, G. Yan, W. Zhao, L. Wang, G. Sun, F. Yang, and Y. Zeng, Appl. Phys. Lett. **105** (2014) 122106.
36) C. M. Eichfeld, M. A. Horsey, S. E. Mohney, A. V. Adedeji, J. R. Williams, Thin Solid Films, **485** (2005) 207.
37) R. P. Devaty, D. J. Larkin, and S. E. Saddow, Mater. Sci. Forum, **527** (2006) 883.

38) R. S. Okojie, A. A. Ned, A. D. Kurtz, and W. N. Carr, IEEE Trans. Electron Devices, **46** (1999) 269.
39) W. Daves, A. Krauss, V. Haublein, A. J. Bauer, and L. Frey, Mater. Sci. Forum, **717** (2012) 1089.
40) T. Marinova, A. K. -Georgieva, V. Krastev, R. Kakanakov, M. Neshev, L. Kassamakova, O. Noblanc, C. Arnodo, S. Cassette, and C. Brylinski, Mater. Sci. Eng. B **46** (1997) 223.
41) S. Tanimoto, K. Watanabe, H. Tanizawa, K. Matsui, and S. Sato, Smart Processing Society for Materials, Environment & Energy, **2** (2013) 144 [in Japanese].
42) A. M. Cowley and S. M. Sze, J. Appl. Phys. **36** (1965) 3212.
43) F. Dadabhai, F. Gaspari, S. Zukotynski, and C. Bland, J. Appl Phys. **80** (1996) 6505.
44) A. Scorzoni, F. Moscatelli, A. Poggi, G. C. Cardinali, and R. Nipoti, Mater. Sci. Forum, **457-460** (2004) 881.
45) L. Huang, B. Liu, Q. Zhu, S. Chen, M. Gao, F. Qin, and D. Wang, Appl. Phys. Lett. **100** (2012) 263503.
46) G. J. van. Gurp, J. L. C. Daams, A. van Oostrom, L. J. M. Augustus, and Y. Tamminga, J. Appl. Phys. **50** (1979) 6915.
47) W. Song, M. Yoshitake, Applied Surface Science **251** (2005) 14.
48) J. Bardeen, Phys. Rev. 71 (1947) 717.
49) A. M. Cowley, and S. M. Sze, J. Appl. Phys. 36 (1965) 3212.

Figure Captions

Table I. (black and white) Specification of contact in cross-bridge kelvin resistors.

Fig. 1. (black and white) (a) Plan view of NN05 and (b) cross section of a cross-bridge kelvin resistor.

Fig. 2. (black and white) (a) Plan view of PP10 and (b) cross section of a cross-bridge kelvin resistor. Plan view is shown together with basic experimental setup, which is the same for NN05.

Fig. 3. (black and white) SMU1 current (I_{SMU1}) and specific contact resistance of NN05 for SMU1 voltage (V_{SMU1}) with SMU2 voltage = 0 V at room temperature. ρ_c is average of contact resistance from -1 V to 1 V except 0 V.

Fig. 4. (black and white) Cross section of a packaged cross-bridge kelvin resistor used for long-term thermal-stability tests in air.

Fig. 5. (black and white) Temperature sequence of thermal-shock test.

Fig. 6. (black and white) Normal distribution of wire's peel-fracture strength before and after thermal-shock test.

Fig. 7. (black and white) Temperature dependence of specific contact resistance ρ_c for (a) NN05 and (b) PP10 before the high-temperature-storage test. The carrier transport is governed by a field-emission (FE) model in case (a) and by a thermionic-field-emission (TFE) model in case (b).

Fig. 8. (black and white) X-ray diffraction spectra of the nickel silicide metal in PP10.

Fig. 9. (black and white) Comparison of specific contact resistance ρ_c for (a) NN05 and (b) PP10 as function of thermal-storage aging time at 300°C in vacuum and 400°C and 500°C in nitrogen atmosphere. ρ_c of the samples heated at 400°C and 500°C test is periodically sampled at room temperature. In contrast, ρ_c of the sample heated at 300°C test is continuously measured by probe. Initial ρ_c of NN05 is 2.8×10^{-6} Ωcm^2 at room temperature and 1.7×10^{-6} Ωcm^2 at 300°C. On the other hand, initial ρ_c of PP10 is 5.8×10^{-2} Ωcm^2 at room temperature and 2.1×10^{-3} Ωcm^2 at 300°C.

Fig. 10. (color online) TEM images of PP10 (a) before and (b) after high-temperature-storage test at 500°C and aging time of 575 hr in nitrogen atmosphere.

Fig. 11. (black and white) (a) TEM-EDX result and (b) enlarged it. These results are at insulator layer after high-temperature-storage test (point 1 in Figure 10(b)).

Fig. 12. (black and white) (a) TEM-EDX result and (b) enlarged it. These results are at contact metal after high-temperature-storage test (point 2 in Figure 10(b)).

Fig. 13. (black and white) (a) TEM-EDX result and (b) enlarged it. These results are at aluminum layer near TiN after the high-temperature-storage test (point 3 in Figure 10(b)).

Fig. 14. (black and white) Specific contact resistance ρ_c of NN05 and PP10 as function of thermal-storage aging time at 300°C in air. Each ρ_c was measured at room temperature at 200-hr intervals. Reported ρ_c for a device with Ni-based ohmic contact to n-type SiC is also shown for comparison[33)]. Initial ρ_c of NN05, PP10 and the device in Ref. 33 are 2×10^{-5} Ωcm^2, 6×10^{-2} Ωcm^2, and 3×10^{-4} Ωcm^2 respectively.

Fig. 15. (black and white) Specific contact resistance ρ_c versus number of thermal-shock cycles for NN05 and PP10 at ΔT= 340°C in air. Each ρ_c was measured at room temperature at almost-the-same time intervals. Initial ρ_c of NN05 and PP10 are 2×10^{-5} Ωcm^2 and 6×10^{-2} Ωcm^2 respectively.

Table I. (black and white) Specification of contact in cross-bridge kelvin resistors.

name	conduction type	concentration (cm^{-3})	contact area (μm)
NN05	n-type	1.0×10^{20}	5 × 5
PP10	p-type	0.7×10^{20}	10 × 10

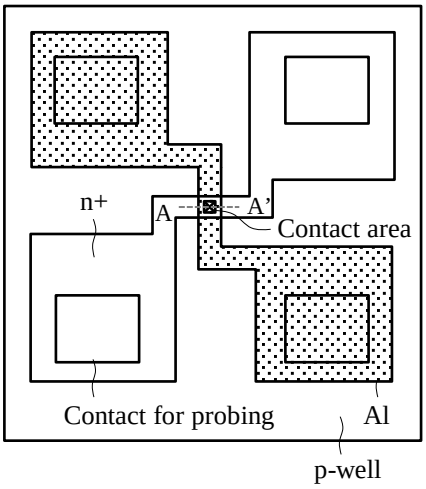

(a)

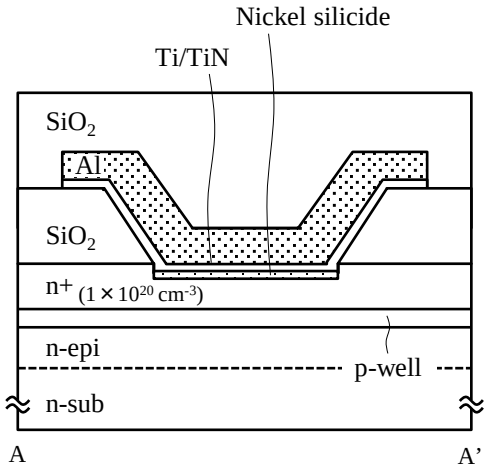

(b)

Fig. 1. (black and white) (a) Plan view of NN05 and (b) cross section of a cross-bridge kelvin resistor.

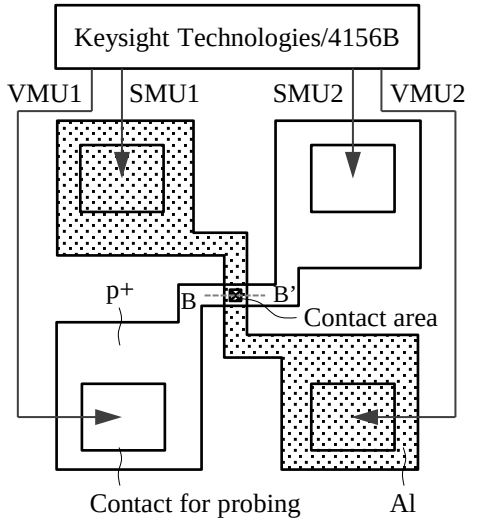

(a)

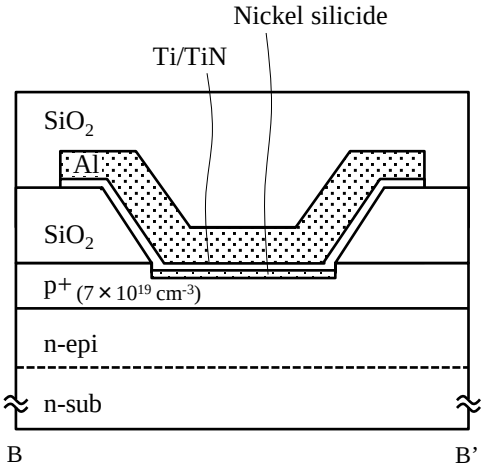

(b)

Fig. 2. (black and white) (a) Plan view of PP10 and (b) cross section of a cross-bridge kelvin resistor. Plan view is shown together with basic experimental setup, which is the same for NN05.

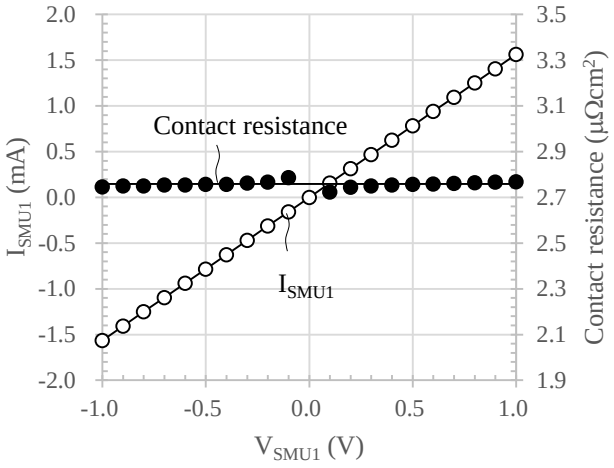

Fig. 3. (black and white) SMU1 current (I_{SMU1}) and specific contact resistance of NN05 for SMU1 voltage (V_{SMU1}) with SMU2 voltage = 0 V at room temperature. ρ_c is average of contact resistance from -1 V to 1 V except 0 V.

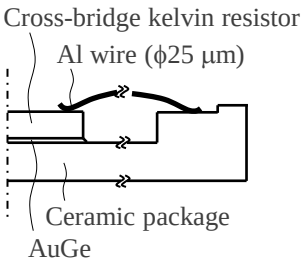

Fig. 4. (black and white) Cross section of a packaged cross-bridge kelvin resistor used for long-term thermal-stability tests in air.

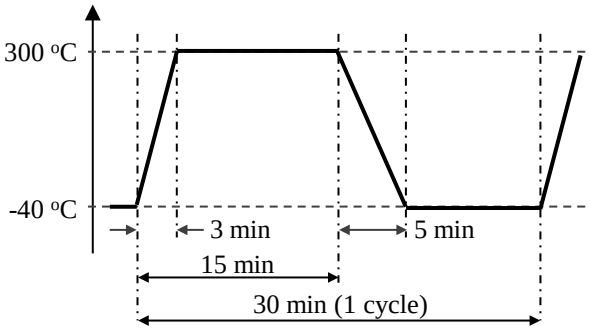

Fig. 5. (black and white) Temperature sequence of thermal-shock test.

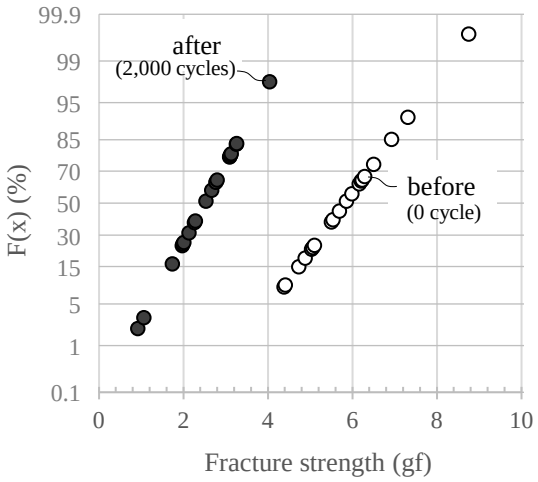

Fig. 6. (black and white) Normal distribution of wire's peel-fracture strength before and after thermal-shock test.

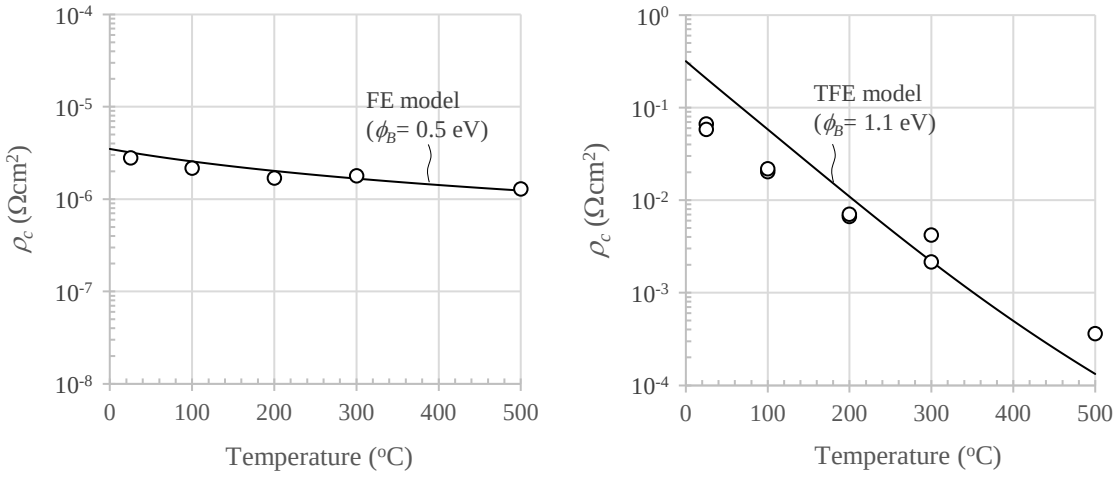

(a) (b)

Fig. 7. (black and white) Temperature dependence of specific contact resistance ρ_c for (a) NN05 and (b) PP10 before the high-temperature-storage test. The carrier transport is governed by a field-emission (FE) model in case (a) and by a thermionic-field-emission (TFE) model in case (b).

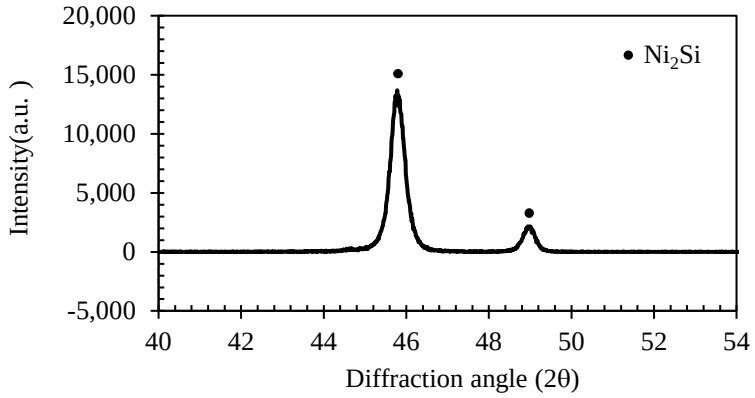

Fig. 8. (black and white) X-ray diffraction spectra of the nickel silicide metal in PP10.

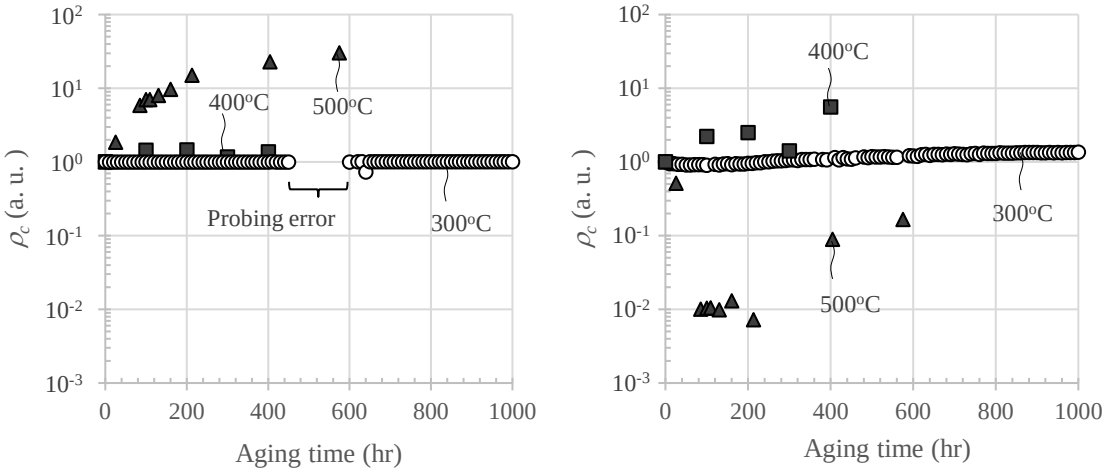

(a) (b)

Fig. 9. (black and white) Comparison of specific contact resistance ρ_c for (a) NN05 and (b) PP10 as function of thermal-storage aging time at 300°C in vacuum and 400°C and 500°C in nitrogen atmosphere. ρ_c of the samples heated at 400°C and 500°C test is periodically sampled at room temperature. In contrast, ρ_c of the sample heated at 300°C test is continuously measured by probe. Initial ρ_c of NN05 is 2.8×10^{-6} Ωcm^2 at room temperature and 1.7×10^{-6} Ωcm^2 at 300°C. On the other hand, initial ρ_c of PP10 is 5.8×10^{-2} Ωcm^2 at room temperature and 2.1×10^{-3} Ωcm^2 at 300°C.

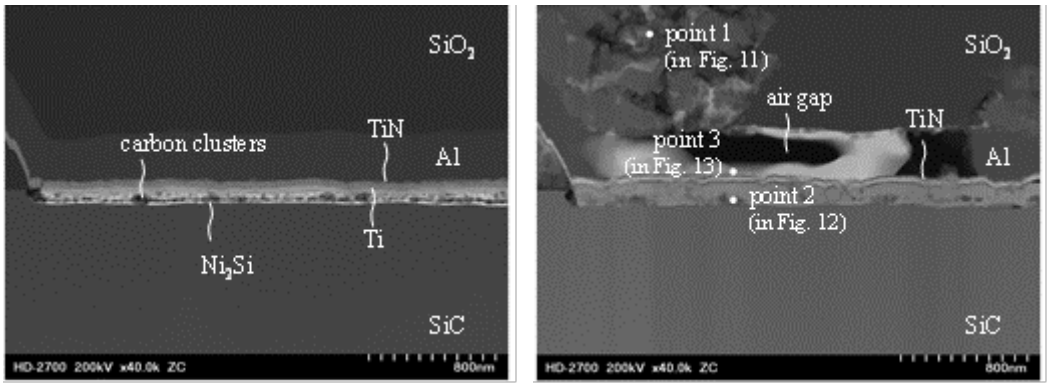

(a) (b)

Fig. 10. (color online) TEM images of PP10 (a) before and (b) after high-temperature-storage test at 500°C and aging time of 575 hr in nitrogen atmosphere.

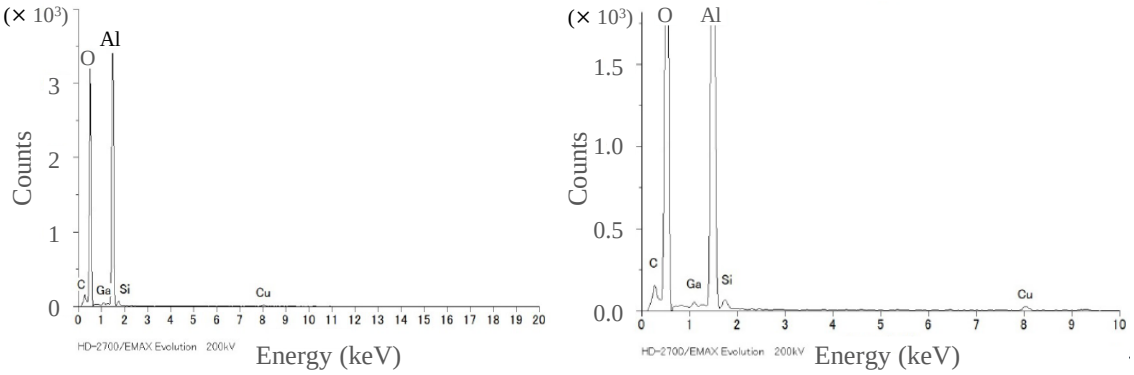

(a) (b)

Fig. 11. (black and white) (a) TEM-EDX result and (b) enlarged it. These results are at insulator layer after high-temperature-storage test (point 1 in Figure 10(b)).

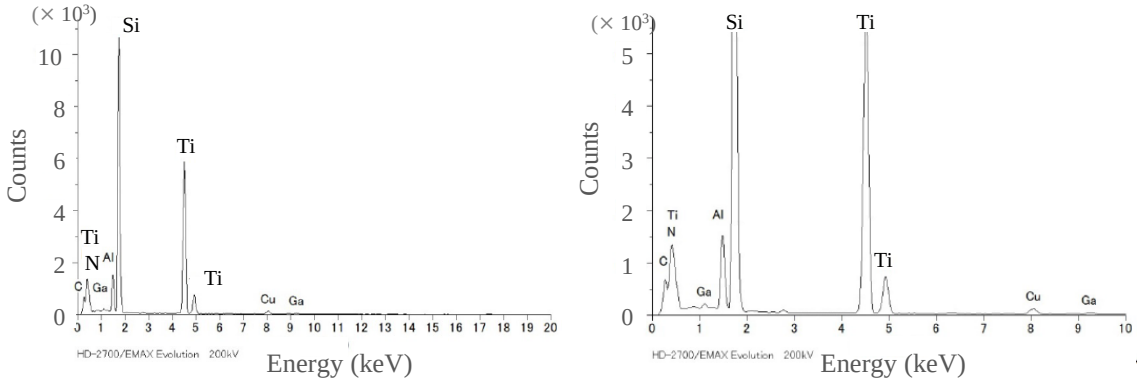

(a) (b)

Fig. 12. (black and white) (a) TEM-EDX result and (b) enlarged it. These results are at contact metal after high-temperature-storage test (point 2 in Figure 10(b)).

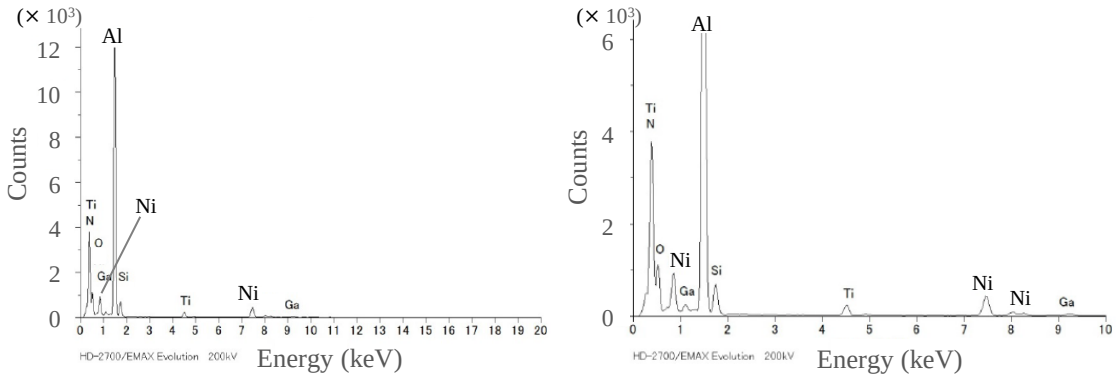

(a) (b)

Fig. 13. (black and white) (a) TEM-EDX result and (b) enlarged it. These results are at aluminum layer near TiN after the high-temperature-storage test (point 3 in Figure 10(b)).

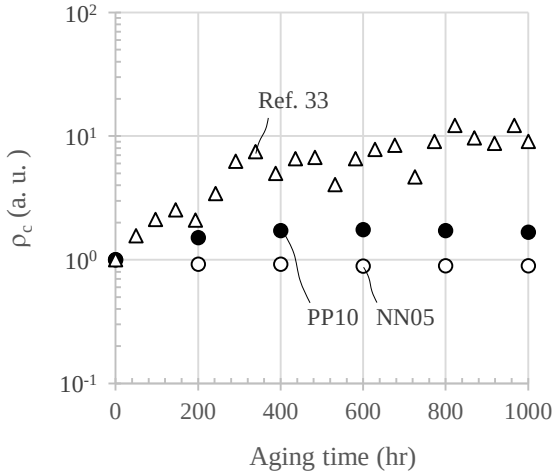

Fig. 14. (black and white) Specific contact resistance ρ_c of NN05 and PP10 as function of thermal-storage aging time at 300°C in air. Each ρ_c was measured at room temperature at 200-hr intervals. Reported ρ_c for a device with Ni-based ohmic contact to n-type SiC[33] is also shown for comparison. Initial ρ_c of NN05, PP10 and the device in Ref. 33 are 2.8×10^{-5} Ωcm^2, 5.8×10^{-2} Ωcm^2, and 3.2×10^{-4} Ωcm^2 respectively.

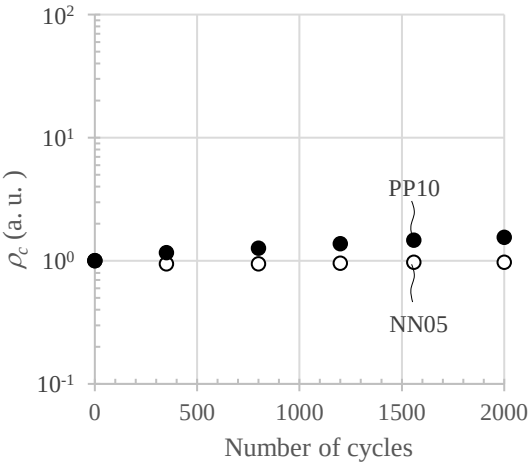

Fig. 15. (black and white) Specific contact resistance ρ_c versus number of thermal-shock cycles for NN05 and PP10 at ΔT= 340°C in air. Each ρ_c was measured at room temperature at almost-the-same time intervals. Initial ρ_c of NN05 and PP10 are 2×10^{-5} Ωcm^2 and 6×10^{-2} Ωcm^2 respectively.